IEEE Access
Multidisciplinary | Rapid Review | Open Access Journal

Received March 26, 2021, accepted April 13, 2021, date of publication April 22, 2021, date of current version May 3, 2021.

Digital Object Identifier 10.1109/ACCESS.2021.3075060

Evaluation of a Planar Reconfigurable Phased Array Antenna Driven by a Multi-Channel Beamforming Module at Ka Band

ALFONSO TOMÁS MURIEL-BARRADO, JORGE CALATAYUD-MAESO, (Student Member, IEEE), ANTONIO RODRÍGUEZ-GALLEGO, PABLO SÁNCHEZ-OLIVARES, JOSÉ MANUEL FERNÁNDEZ-GONZÁLEZ, (Senior Member, IEEE), AND MANUEL SIERRA-PÉREZ, (Life Senior Member, IEEE)

Centro de Investigación en Procesado de la Información y Telecomunicaciones, ETSI Telecomunicación, Universidad Politécnica de Madrid, 28040 Madrid, Spain

Corresponding author: Pablo Sánchez-Olivares (pablo.sanchezo@upm.es)

This work was supported in part by the Spanish Government, Ministry of Economy, National Program of Research, Development and Innovation through the Project FUTURE RADIO ''Radio systems and technologies for high capacity terrestrial and satellite communications in an hyperconnected world'' under Grant TEC2017-85529-C3-1-R, and in part by the Project JETSTREAM ''Desarrollo de una antena banda KA embarcada para la prestación de servicios de acceso a Internet por satélite en aviación comercial'' in collaboration with TELNET Redes Inteligentes S.A. under Grant RTC-2015-3495-7.

ABSTRACT In this paper, a planar active phased array antenna demonstration with linear polarization (LP) at Ka Band (28-30 GHz) is presented. The proof of concept is carried out to evaluate the possible problems that may arise, to analyze possible calibration stages and to assess the viability of the integration of an active system with a Multi-Channel Beamforming Module (MCBM). To fulfill this task an 8 × 8-element planar array arranged in column subarrays of 1 × 8 elements for 1D beam steering is proposed. The single element consists of a printed circular patch connected to a microstrip feeding line through metallic vias in a multilayered structure. Both the amplitude and phase distributions are performed by a commercial integrated circuit (IC) designed for transmission purposes, from the common port to each of the 8 output ports. Thus, an evaluation of the IC performance is also included within this work. Despite the inherent amplitude and phase feeding errors of the IC, the beam-steering accuracy of the system is reasonable. A nice correspondence between the simulated and measured 8 × 8-element array beam steering directions is obtained, with errors below 1° in the steering of the beam.

INDEX TERMS Active phased array, beam steering, antenna integrated circuit, Ka band antenna.

I. INTRODUCTION

Nowadays, the need for higher data transmission rates demanded by communication systems such as satellite communications (SATCOM) [1]–[3] and 5G applications [4]–[6], or the increasing in versatility experimented by radar systems [7] is leading to different design trends of beam-steered antennas at higher frequencies, whose challenges may differ from each other depending on the particular application or segment.

A lot of SATCOM On-The-Move (SOTM) solutions for the ground segment are reported in literature such as reflector, reflectarray, transmitarray and lens antennas that combines different design approaches to obtain beam steering capabilities. Typically, this type of application makes use of the frequency band between 18 GHz and 20 GHz and the band between 28 GHz and 30 GHz for the reception and transmission systems, respectively. These frequency bands offer better bandwidth behavior than lower frequency bands, as well as electrically bigger antenna surface for the same physical dimensions.

Firstly, reflector antennas are commonly used in a dual reflector configuration together with a phased array feeder forming what is known as a Focal-Plane Array (FPA) [8]–[10]. This is a versatile solution that may overcome the speed problem of mechanical beam steering [11] or achieve operation in several frequency bands [12]. Secondly, reflectarray antennas also provide a huge range of design alternatives that include dual-band [13], dual-polarization [14]–[16] or wide scanning angle [16], [17]

The associate editor coordinating the review of this manuscript and approving it for publication was Qi Luo.

behavior. Besides, transmitarray antennas may fulfill the same requirements with a more compact structure [18]–[22]. With regard to lens antennas, they are implemented in both dielectric [23], [24] and planar [25], [26] technology and they usually require mechanical control to modify the beam. Nevertheless, all these solutions do not show low profile features, which are desirable for SOTM applications since they require structures as aerodynamic as possible. Therefore, planar phased array antennas seem to be a suitable solution to perform an aerodynamical steering of the beam.

Since mechanical orientation in the two axes (2D) of the antenna [1], [20], [23]–[26] does not meet low-profile properties for the entire system, many solutions tend to combine electronic and mechanic means (1D), one per axis of the antenna [1], [12], [14] or to develop a complete electronic control of the beam [2]–[4], [14], [16], [18], [19]. Besides, 2D mechanical beam steering is unsuitable for rapid variation scenarios, and any possible mechanical control (1D or 2D) malfunction may be critical for the system performance while an electronic misfunction may only affect to several radiating elements. Thus, the current design trend is towards fully electronic reconfiguration schemes for planar phased array antennas [27]–[39], [42], [43], despite they increase the complexity of the feeding network and its associated control circuitry.

The phase shifting for the electronic reconfiguration of the beam in planar phased arrays could be applied by means of very different discrete elements. PIN diodes [27] usually offer a cost-effective solution in spite of the losses they present. On the contrary, varactor diodes [28], [29] present a low-loss option with the same low-cost characteristics. Nevertheless, a diode-based option usually requires sufficient space to make integration at element level extremely difficult for 2D planar arrays. A very promising solution to cope with these integration requirements are the System-on-Chip (SoC) or Integrated Circuit (IC) devices. The state-of-the-art SoC solutions bring together different kind of fabrication processes such as GaAs, CMOS or Si/SiGe BiCMOS for RF purposes [40]. SoCs may also incorporate radio-frequency microelectromechanical systems (RF-MEMS) for switching [41], phase delaying [42] or capacitance tuning [43]. When the SoC implements different RF/mmW circuitry it receives the name of Monolithic Microwave Integrated Circuit (MMIC's). They are able to integrate RF components (including RF-MEMS [40]) in such a high-density manner that different RF architectures may be performed within the same IC, like multi-channel transceiver chains [38], [39] or phased-array front-ends [45]. For last, the antenna system may be embedded in the SoC, which is reported in literature as Antenna-on-Chip (AoC) or Antenna in Package (AiC), depending on the integration scheme [46]. Nevertheless, this approach is not suitable for very large antenna structures where scalability and efficiency are major issues.

As it can be seen, there are a lot of possible combinations of different technologies or architectures to implement RF/mmW devices. For phased-array purposes, the abovementioned front ends [45] seem to be a really good choice when scalable, high-density, low-profile, high-speed beam-steering properties are desired. Furthermore, several commercial ICs designed for the reception system (from 18 GHz to 20 GHz) and for the transmission system (from 28 GHz to 30 GHz) are available on the market to develop SOTM antenna systems. They consist of several independent channels from a common port with discrete Amplitude Control (ACt) and Phase Control (PCt) per channel. That is why they are also known as Beamforming Modules (BM) [34] or Multi-Channel Beamforming Modules (MCBM) [35]. Furthermore, due to the versatility they add, other properties such as Sidelobe Level (SLL) and polarization control may be obtained. Thus, this design approach is setting the trend for current planar phased-array systems.

Nevertheless, a lot of MCMB-driven planar phased array antennas reported in literature [30], [31], [33]–[38] do not analyze neither the behavior of the IC and its non-idealities nor its direct impact on the radiation properties of the array when both are integrated. However, it is true that many other papers employ numerous mathematical analysis techniques to infer the effects of devices such as amplifiers or phase shifters on the radiation pattern. For example, in [47] a 4-element printed linear array with a beamforming novel technique, which uses a single ACt and a single phase shifter for the entire array, is analyzed. Moreover, it includes one additional amplifier for each radiating element, which is characterized by a frequency-dependent non-linear behavioral model. With a one-tone and two-tone signal description the proposed analysis is capable of predicting the behavior of the entire array antenna. Other techniques such as the application of the non-linear Shimbo model [48], which takes into account the memory effects of the power amplifiers, and other circuit model approaches [49], [50] have been proposed by authors to characterize active array antennas. Nevertheless, such techniques becomes extremely hard to apply to MCMB-driven antennas for several reasons. In these analytical works, the active components associated with the antenna are known, whereas in MCMB-driven antennas, the particular layout of the utilized IC is unknown. For high-frequency purposes (as in the present work), it becomes extremely difficult to make room for active devices such the ones proposed in some of the references [47]–[50]. Thus, MCMB modules are of great relevance, and an analytical approach of a different active antenna scheme is also discarded. In addition, and as it will be covered below, these MCMB modules are sufficiently complex (with dependencies between PCt and ACt and between channels) that an analytical characterization based on empirical measurements may not be feasible. Consequently, as a preliminary step, the integration stage between the antenna and the MCMB module is analyzed, prior to a more rigorous mathematical characterization. In addition, the integration stage means a key factor to analyze the potential problems of the system or the possible calibration requirements that will assess the viability of such type of systems. With this work, a lot of applications may benefit from an agile and ease

design and manufacturing process, since a calibration stage may be unsuitable for very large aperture antennas that make use of MCMB modules. Besides, this work estimates the loss in performance that the active antenna system may suffer.

This analysis approach is followed experimentally throughout the present paper with a proof of concept that works at Ka Band (28-30 GHz). For this purpose, the AWMF-0109 commercial IC from Anokiwave is used. This IC is a MCBM with 8 independent channels with 5-bit PCt and ACt. The commercial evaluation kit of the IC is then used to evaluate the integration step of the IC with the proposed planar antenna. Cables and coaxial-to-microstrip transitions are also necessary to interconnect both the antenna and the active device. Hence, the effects of these parts on the system performance should be characterized and calibrated. The planar array antenna is supposed to validate the beam-steering accuracy achievable with this IC and to analyze the viability of the complete active system. A 8 × 8-element array arranged in 8 corporately-fed subarrays of 1 × 8 elements for linear polarization (LP) 1D beam-steering is proposed.

It is well known that satellite communications use antennas with circular polarization and not linear polarization. However, in order to achieve SOTM capabilities the antenna has to be able to generate switchable circular polarization. Consequently, the radiating elements require a dual-feeding scheme to control not only the phase of the element, but also the phase difference between ports to obtain left-handed or right-handed circular polarization. With this architecture, a single IC would drive an array of up to 4 elements, typically arranged in a 2D squared grid. Each IC output port would be attached to one of the two radiating element inputs. Hence, either the radiators are single elements or larger subarrays, the viability of the system becomes really hard to analyze. In the first case, the main beam produced by the antenna would be very wide, so even for little beam-steered angles it gets very difficult to assess where the antenna is actually pointing. In the second case, only 2 elements are controlled no matter the size of the antenna or the axis in which the pointing is to be performed. For this reason, if the radiation properties of a switchable circularly polarized array need to be analyzed, more than one IC should be used. Thus, the analysis of a single IC is not possible, and the degree of uncertainty increases in the analysis since more than one IC would be tested at once.

With the proposed design the steering may be tested with a narrow and well-defined beam. Switchable circular polarization is replaced by linear polarization in order to control a bigger number of radiating elements or in this case subarrays. Specifically, one subarray for each port in the IC, which leads to a more straightforward analysis. It is important to highlight that the proposed analysis, calibration scheme and the achieved results may differ for other type of antennas, such as those that perform the switchable circular polarization, as it will be discussed in the next sections. Since the proposed proof-of-concept is dealing with low-profile integration issues, the radiating elements are circular printed patches connected to microstrip feeding lines by means of metallic vias. For final integration and scalability other transmission lines like stripline may be suiter, but this way it is much easier to perform the proposed analysis. The reason behind the shape of the radiating elements is to develop a switchable circular polarization analysis in further research steps with other radiating structures.

II. PROOF-OF-CONCEPT DESCRIPTION

The proposed proof-of-concept at Ka band (28-30 GHz) is depicted in Fig. 1. It results from integrating the IC Evaluation Board (IC-EB) with the board of the array antenna. This integration is performed via Minibend KR-6 cables and Southwest 1092-04A-6 2.92 mm end-launch connectors. Thus, the potential transmission imperfections of such components should be taken into account in the integration process and should be calibrated and compensated as much as possible through the IC ACt and PCt.

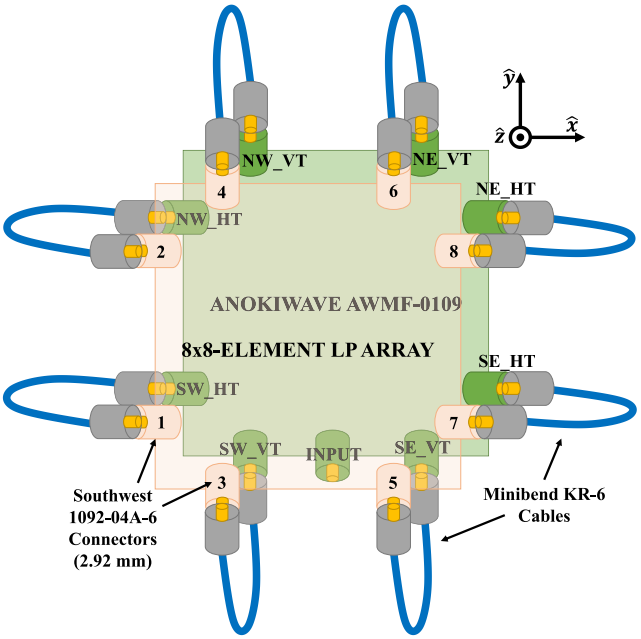

FIGURE 1. Proposed proof-of-concept integration scheme.

The IC-EB scheme is shown in Fig. 2. It interconnects the 8 output ports and the common input port of the IC with the corresponding 2.92 mm coaxial terminals of the IC-EB. This connection is performed by means of grounded coplanar waveguides (G-CPW), which are more suitable for soldering this kind of ICs. As it can be appreciated, every output port is labeled with its geographical position in relation to the center: N for North, S for South, E for East and W for West. The name also includes the virtual polarization each port would control for other kind of dual-polarized radiating structures: VT for Vertical Transmit and HT for Horizontal Transmit. This fact reveals that this kind of ICs are meant to be used in other kind of radiating structures (such as 2 × 2-element

dual-polarized subarrays), as discussed above. Nevertheless, with the proposed analysis the characterization and viability assessment of a single-IC integration scheme in terms of beam steering is not only easier, but possible. The IC-EB also contains all the required hardware and software to control the IC from a PC. Nevertheless, a proprietary tool has been developed to automate the measurement process not only for the IC-EB with a VNA but also for the measurement of the proof-of-concept in the anechoic chamber.

Fig. 2 not only shows the general scheme of the IC-EB, but it also provides an idea of the block diagram of the IC. It offers 8 different and independent paths where a 5-bit ACt may be applied to the transmitted signals, with a Less Significant Bit (LSB) value of 0.5 dB and a dynamic range of 15 dB. Furthermore, a PCt with a LSB of 11.25° is available. Several temperature and gain compensation amplification stages are also included at the common branch. It is important to highlight that the AWMF-0109 is a commercial device, so the particular block diagram of the IC is unknown.

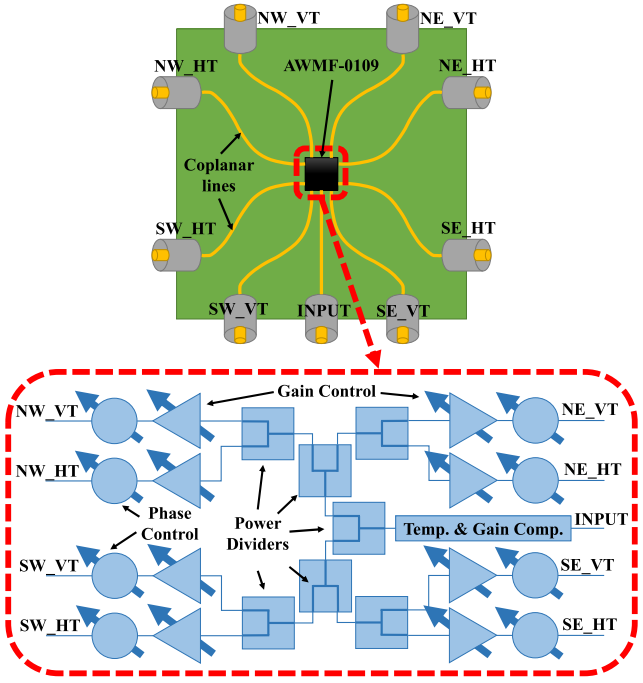

FIGURE 2. Integrated Circuit (IC) evaluation board and block diagram.

A scheme of the proposed planar array antenna appears in Fig. 3. It consists of a 8×8-element Linearly Polarized (LP) circular printed patch array. This aperture is arranged in 1 × 8-element corporately-fed column subarrays. Therefore, depending on the phase difference among the input ports, an azimuth beam steering may be performed. The radiating element of the proof-of-concept is in this case vertically polarized. Each input port is named from 1 to 8 from the left column to the right column when it is seen from the front.

The radiating element is fed from the opposite layer by microstrip transmission lines. Then, patches and lines are connected through metallic vias passing through an

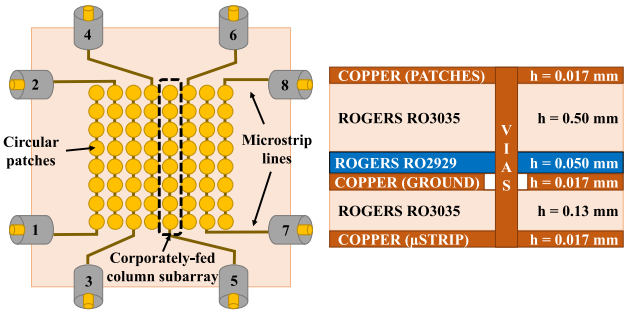

FIGURE 3. Scheme of the proposed 8 × 8-element planar array antenna for azimuth beam steering with its corresponding stack-up.

intermediate ground plane by means of circular apertures. All the corporate feeding network input lines end up in a transition to the 2.92 mm Southwest connector. Additionally, several intermediate prototypes were manufactured to verify design process. Of course, all these designs were performed in the same frequency band of the IC (28-30 GHz).

Finally, in Fig. 3 it is also depicted the stack-up of the antenna. A Rogers RO3035 substrate is used for the patches and for the microstrip lines. It presents an $\varepsilon_r = 3.50$ and a $\tan\delta = 0.0015$ at 10 GHz. To attach both substrates, a Rogers RO2929 prepreg is employed. It presents an $\varepsilon_r = 2.94$ and $\tan\delta = 0.003$ at the same frequency.

III. PASSIVE ARRAY ANTENNA DESIGN AND MEASUREMENT

In this section, passive array antenna design, manufacture and measurement steps are discussed.

A. PASSIVE ARRAY ANTENNA DESIGN

Fig. 4(a) depicts the 8 × 8-element proposed design as viewed from the front. All the radiating elements are arranged in 1×8-element column subarrays, all of them fed by a corporate microstrip feeding network located on the opposite side of the board (see Fig. 4(b)). Each of the networks is connected to one of the eight ports of the prototype. However, this design is limited by the separation between elements dx since it determines the space available for the corporate microstrip feeding networks. This fact could lead to mutual coupling among different microstrip lines that may disturb the radiation pattern of the array. In Fig. 4(c)-(d) it may be appreciated respectively a detail view of the 8 × 8-element array and the set of 8 corporate microstrip feeding networks.

Regarding the radiating elements, the proposed antenna uses circular printed patches fed by the microstrip transmission lines of the corporate feeding networks. Both of them are connected by metallic vias. This connection is made through a circular aperture performed on the ground plane between them. Fig. 4(e)-(f) show, respectively, a detailed view of the vertically polarized radiating element from the front and from the back. The stack-up has been made transparent within Fig 4(e)-(f) to better display the multi-layered structure of the circular patch. For linear polarization, rectangular patches may be suiter, but circular patches are

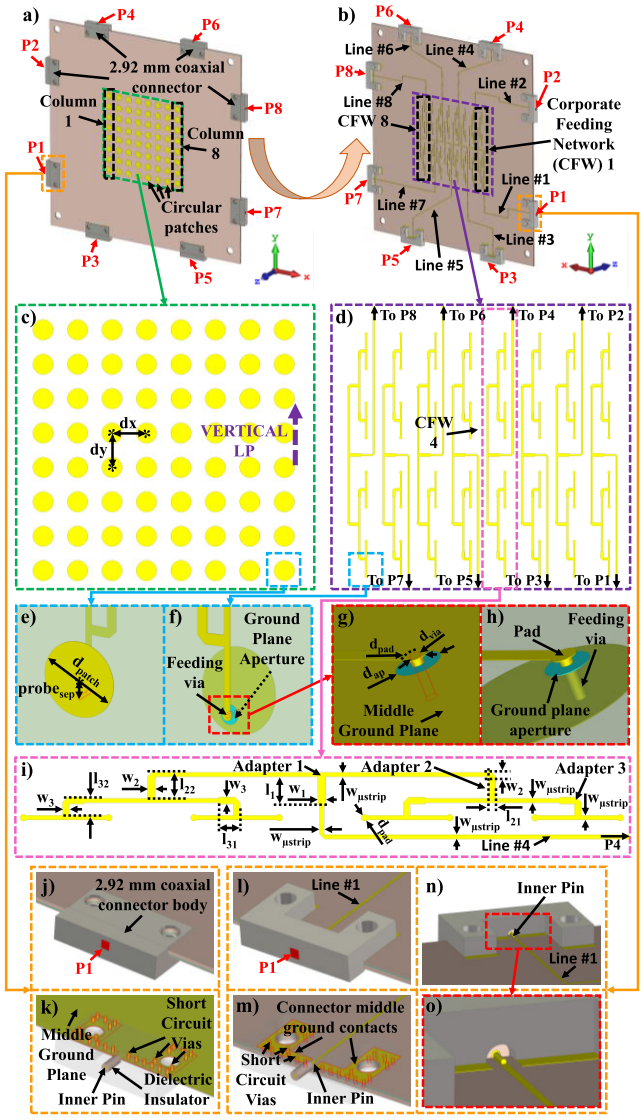

FIGURE 4. Linearly polarized 8 × 8-element circular printed patch array antenna prototype: (a) front view, (b) back view, (c) 8 × 8-element array (detail), and (d) corporate feeding network array (detail). Circular printed patch element: (e) front view, and (f) back view (all the stack-up is hidden). Microstrip to patch metallic via transition detail view: (g) with the microstrip feeding lines substrate hidden, and (h) with all the stack-up hidden. (i) Corporate feeding network 4 detail view. Southwest 1092-04A-6 2.92 mm coaxial connector: (j) front view as seen from the port, (k) front view as seen from the port (patches substrate and connector body are hidden), (l) back view as seen from the port, (m) back view as seen from the port (connector body is hidden), (n) back view as seen from the feeding line, and (o) back view as seen from the feeding line (detail). Design dimensions in mm are $d_{patch} = 3.06$, $d_{ap} = 0.7$, $d_{via} = 0.2$, $d_{pad} = 0.4$, $probe_{sep} = 0.75$, $dx = dy = 0.5 \cdot \lambda_0$ (@ 29 GHz) $= 5.17$, $w_{ustrip} = 0.26$, $w_1 = 0.48$, $l_1 = 1.67$, $w_2 = 0.45$, $l_{21} = 0.5$, $l_{22} = 1.65$, $w_3 = 0.4$, $l_{31} = 1.3$, and $l_{32} = 1.1$.

used in order to develop future research steps with the analysis of the IC performance in terms of axial ratio. Moreover, in Fig. 4(g) it can be appreciated a detailed view of the metallic via transition between the patches and the feeding lines with the patches microstrip lines substrate hidden to make the intermediate ground plane visible. Fig. 4(h) shows the same via transition view but with all the stack-up hidden. Since the relative bandwidth of the defined frequency band is around 7% this feeding method is enough to maintain the structure matched. Besides, a single patch configuration instead of a double-stacked patch structure has been used for the proposed proof of concept.

Additionally, a detailed view of the corporate microstrip feeding network together with its main dimensions is shown in Fig. 4(i). It can be observed the three different division levels with their corresponding $\lambda/4$ transformer. Depending on the division level, the particular transformer is bended at a different point in order to mitigate as much as possible the mutual coupling effects between lines. Finally, Fig. 4(j)-(o) show three different figure subsets with the connector model and its transition to the microstrip line from different points of view. The first subset (Fig. 4(j)-(k)) depicts the connector transition viewed from the front of the antenna and from the input port. Since the patches substrate and the connector body are hidden, in Fig. 4(k) it can be appreciated the intermediate ground plane and short-circuiting vias that interconnect it to the transition. The second subset (Fig. 4(l)-(m)) represents the connector transition viewed from the back of the antenna and from the port. In the case of Fig. 4(m) only the body connector is hidden, exposing the transition structure and the transition contacts to the intermediate ground plane. The third subset (Fig. 4(n)-(o)) displays the transition viewed from the back of the antenna and from the microstrip line. In Fig. 4(o) the place where the inner pin of the coaxial connector and the microstrip line make contact is magnified.

Concerning the way in which the antenna is fed, the IC will deliver a frequency-dependent complex feeding coefficient $A_n = a_n \cdot e^{j \cdot \alpha n}$ to each column subarray of the antenna n, with $n = 1, \ldots, 8$. Regardless of the potential errors the IC would introduce in these coefficients, the steering of the beam might be achieved by varying the phase α_n among the different columns in such a way that the aperture field phase approach a linear function with minimum error. This condition should remain unaltered no matter the absolute phase value of each element. This phase variation is called the progressive phase shifting and it is defined as $\alpha_n = \alpha_0 - n \cdot \varphi$, with $n = 1, 2, \ldots, 8$, and α_0 being an arbitrary value. Consequently, a 1D azimuth steering of the beam is established by varying this progressive phase shifting φ among column subarrays. An amplitude distribution to reduce the Sidelobe Level (SLL) parameter may be also applied to the radiation pattern by modifying $a_1, a_2, \ldots, a_8$ coefficients.

Finally, the frequency dependence of the coefficients A_n together with the errors in the transmission parameters introduced by the IC should be taken into account when characterizing the IC to decide if a calibration is required. These errors may disturb the radiation pattern of the active array antenna and consequently they may reject the viability of the proposed system.

B. PASSIVE ARRAY ANTENNA FABRICATION

The final prototype of the vertically polarized 8 × 8-element array antenna is represented in Fig. 5 (front view and

back view). It can be seen the 8 different subarray columns, with the first and the last one highlighted. Each input port of the design is labeled with its corresponding column. Both of them input port and column are connected by different bended microstrip lines with different shapes, numbered with their respective column and port. The purpose of these lines is to distribute all the 2.92 mm coaxial connectors (also depicted in Fig. 4(a)-(b) and Fig. 4(j)-(o)) around the entire contour of the board while the array antenna is centered. These lines have been designed to measure the same electrical length. An intermediate prototype with all these transmission lines was also considered to characterize any possible fabrication mismatches (Fig. 5(c) and Fig. 5(d)). If this happens, the transmission phase differences among them could lead to undesired effects on the final radiation pattern of the active antenna. Since the IC is able to modify the transmission parameters, this analysis should be used to calibrate the complete integrated system to achieve optimum active performance. Fig. 5(b) shows also the 8 corporate microstrip feeding networks located in the back side of the antenna, where the first and the last one are highlighted. All of them are named with their corresponding column, line and port. The transition to the 2.92 mm coaxial connector is also displayed and it is present in all the input ports of the design.

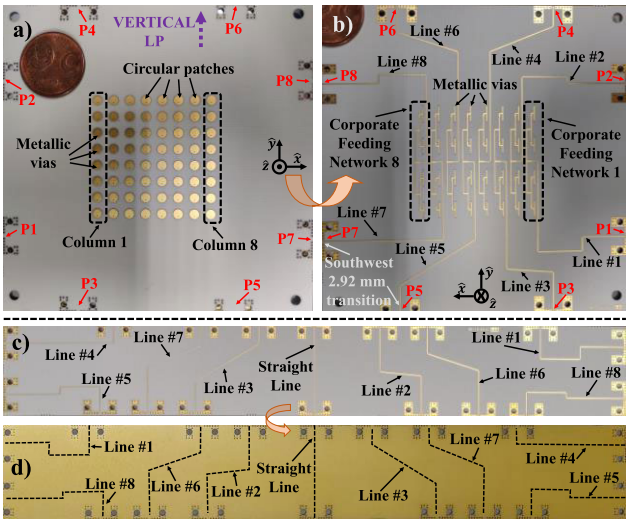

FIGURE 5. Linearly polarized 8 × 8-element array antenna prototype: (a) front view, and (b) back view. Microstrip feeding lines intermediate prototype: (c) front view, and (d) back view.

C. PASSIVE ARRAY ANTENNA MEASUREMENT: S-PARAMETERS AND RADIATION PATTERN

The measured and simulated results of the considered prototype are depicted in Fig. 6. They can be divided into 2 different groups: passive S parameters for the column subarray 4 and active S parameters for some ideal beam-steered directions.

It can be seen that the depicted passive reflection coefficient $|S_{44}|$ in Fig. 6(a) remains below −12 dB for the entire frequency band. In addition, all the reflection coefficients

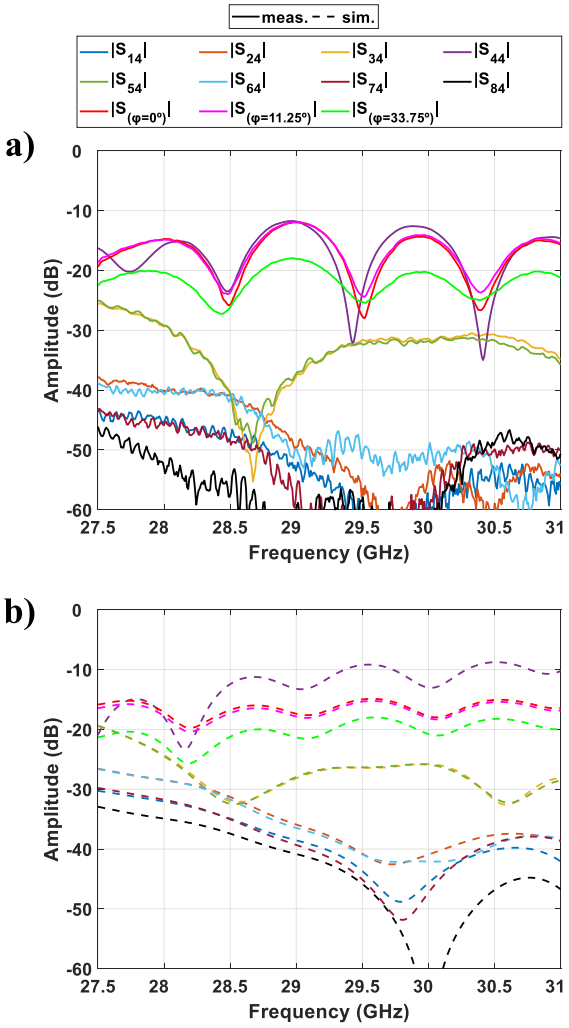

FIGURE 6. (a) Measured, and (b) simulated 8 × 8-element array antenna S parameter results: reflection $|S_{44}|$ and transmission $|S_{X4}|$ for column subarray 4 and active reflection for $\varphi = 0°$, 11.25°, and 33.75°.

of the rest of the column subarrays show similar responses because mutual coupling among columns was taken into account in the design process. This coupling parameter $|S_{X4}|$ is also depicted within Fig. 6(a), and it presents maximum amplitude levels of around −20 dB in the entire frequency band, which are regarded as reasonable values for this kind of structure. Higher mutual coupling values could lead to several undesired effects and imbalances not predicted by the classical array antenna theory. The radiation pattern of the single elements and therefore of the entire array may get distorted due to the surface currents induced by the coupled fields. Thus, the obtained radiation pattern will differ from what would be expected from the theory. In addition, the coupled fields will be translated into a modification of the active impedance (which is described below) at the input port of the array. These changes could provoke the array to be mismatched, and therefore, the Effective Isotropic Radiated Power (EIRP) of the antenna to be downsized. As mentioned hereafter, this decay will not be detected at the input of

the IC. Naturally, the more the mutual coupling, the more the antenna will be mismatched. Besides, mutual coupling between elements could produce very strong decreases in the achieved EIRP for beam-steered systems for certain pointing directions (blind angles). A maximum value of -20 dB of mutual coupling between elements will not significantly affect the antenna performance in terms of the radiation pattern, maximum achievable EIRP or input impedance. If a perfect input impedance matching and a maximum coupling level of -20 dB for the adjacent radiating elements (it can be seen in Fig. 6(a) that for further elements this coupling level remains practically negligible) are considered, the input impedance matching will change to $|\Gamma_{in}| = -13$ dB (assuming these couplings are combined in phase). For other complex additions the input impedance matching level will be below -13 dB. This change in the input impedance will lead to a maximum gain decay of $1 - |\Gamma_{in}|^2 = -0.01$ dB. Therefore, these mutual coupling levels can be neglected for this type of antenna. For other radiating structures this mutual coupling parameter may get higher since more than one linear polarization may be used. Thus, depending on the radiating structure the mutual coupling value may be considered reasonable or not.

Regarding the active S parameters depicted in Fig. 6(a), they represent the reflection coefficient of the proposed antenna prototype for some ideal phase distributions of the IC. These parameters are obtained by combining in simulation all the measured $S_{X,Y}$ parameters for the same Y input port. The output ports X go from 1 to 8, and the ideal phase distribution per pointing direction is set at each port. Once these parameters are calculated, they are combined in simulation again for all the input ports Y, as if they are corporately fed from a common port. The final results for this calculation for both measured S-parameters and simulated S-parameters of the antenna are the ones depicted in Fig. 6(a)-(b). The angle φ is selected as a function of the pointing direction and PCt is set to minimize que aperture phase error. A uniform amplitude distribution ($a_1 = a_2 = \ldots = a_8 = 1$) is considered, like all of the beam-steered states analyzed at the end of the paper. This parameter provides an idea of how these mismatches might affect to the maximum achievable EIRP by the active antenna. Since the integration process does not allow to access to this parameter, and the input reflection coefficient of the complete antenna will be the one at the input of the IC, the performance losses due to passive mismatching may be quantified prior the integration process. So, the active S parameters displayed in Fig. 6(a) (uniformly fed amplitude and with no phase errors) remain below -12 dB. For the beam-steered directions close to the broadside, the response does not deviate from the passive response. For directions away from the broadside this parameter is even lower, so it can be concluded that a sub-optimal active antenna performance is achieved. As it can be appreciated in Fig. 6(a)-(b), the simulated and measured results match reasonably well. The observed discrepancies may be caused by manufacturing defects, insufficient characterization of the materials at 28 GHz - 30 GHz frequency band, buckling of the board due to the asymmetry in the stack-up, and the clearance present between the connectors and the board, which may cause them not to make perfectly centered contact.

Finally, in Fig. 7 it can be seen the radiation properties of the proposed passive array antenna. It shows the comparison between measured and simulated normalized copolar (CP) and crosspolar (XP) radiation patterns at the central frequency of 29 GHz and the extreme frequencies of 28 GHz, and 30 GHz for the 8×8-element prototype, and for the $\phi = 90°$ cut. As it can be appreciated, all the radiation patterns match nicely with what was expected from the simulation results. The response of the array at the other principle cut $\phi = 0°$ is very close to the depicted response for $\phi = 90°$.

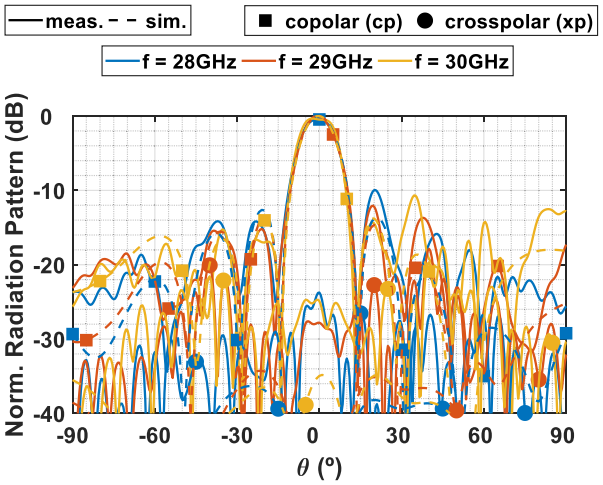

FIGURE 7. Copolar (CP) and crosspolar (XP) normalized radiation patterns at 28 GHz, 29 GHz, and 30 GHz for one column subarray for $\phi = 90°$.

IV. INTEGRATED CIRCUIT CHARACTERIZATION PROCEDURE

This chapter covers the characterization of the active device of the system. Fig. 8(a) physically shows the Anokiwave AWMF-0109 IC-EB. It has the eight output ports and the input port surrounding the board. As previously said in Section II, the eight output ports are labeled with their geographical position with respect to the center and the virtual polarization that they would control if other type of dually polarized structures are connected to them (as it was discussed above): e.g. NW-VT for NorthWest Vertical Transmit port. The IC and its corresponding input/output ports are connected by grounded coplanar waveguide (G-CPW) transmission lines.

The measurement setup is depicted in Fig. 8(b). The IC-EB is connected to the DC power supply and the VNA ports 1 and 2 are respectively connected to the input port and the output port of the channel under test. The rest of the output ports are loaded with 50 Ω coaxial terminations. A software measurement tool that controls the IC and the VNA was developed to automatize the IC characterization process due to the high number of possible configuration states of the IC.

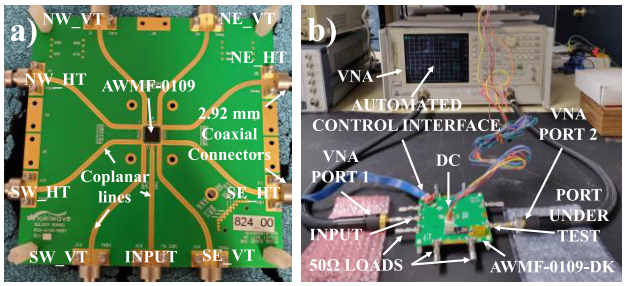

FIGURE 8. **Anokiwave AWMF-0109 IC-EB: (a) front view, and (b) within the measurement setup.**

For example, if a certain amplitude distribution is established, there will be 2^{nbits} possible phase selection for each element, where nbits is the number of bits associated to the PCt. Considering only phases associated to some pointing direction, the number of available directions is very large. Furthermore, if for each phase configuration an ACt is applied, the number of measurements will be even higher. Hence, the software tool automatizes all the measurements for all the defined configuration states. Then, each port is automatically measured for all of the desired configurations, leaving the change of port under test as the only manual operation.

For the S-parameter measurement discussion, a reference configuration state for the IC will be taken. This configuration will be the one that generates the broadside state for the active antenna. The other beam-steered configurations of the system will start from it. Thus, a uniform amplitude distribution with a progressive phase shift of $\varphi = 0°$ is expected from the IC. For this state, Fig. 9(a)-(c) displays the amplitude and phase transmission state of each channel along with their reverse transmission and reflection coefficients, and the input reflection coefficient of the AWMF-0109 IC. Fig. 9(a) depicts the amplitude transmission parameter $|S_{21}|$ per port referenced to SW_HT port. Considering a uniform amplitude distribution, it can be seen that the amplitude error is below ± 1 dB for the worst case within the operational frequency band. This amplitude error is significant and is above the amplitude value of the LSB of the IC. Extensively, the absolute transmission gain for the reference channel is around 18 dB for most of the frequency band. Fig. 9(b), on the other hand, shows the phase transmission parameter $\angle S_{21}$ per port, also referenced to the SW_HT. It can be appreciated that all the channels are reasonably equalized in the phase transmission, with an observed error value close to $\pm 6°$ at 29 GHz. This error is within half the phase value of the LSB of the IC. Moreover, Fig. 9(c) exhibits the reverse amplitude transmission coefficient $|S_{12}|$ per channel, the reverse amplitude reflection coefficient $|S_{22}|$, and the input reflection coefficient $|S_{11}|$ of the IC for this uniformly-fed broadside state. Both the reverse amplitude transmission and reflection parameters are reasonably below -35 dB and -10 dB respectively. However, the input reflection coefficient is slightly worse, with a maximum value of -8 dB. It is important to highlight that the input reflection coefficient of the active antenna will be the one depicted in Fig. 9(c), that is fixed by the IC, and not the active one depicted in Fig. 6(a)-(b). This active input reflection coefficient, which is the one of the passive array antenna for a certain beam-steered state, will downsize the maximum available EIRP of the system without being reflected on the $|S_{11}|$ of the active antenna.

Despite the phase error coming from the IC is relatively low, the amplitude error is considerably high. In fact, it is high enough to try to mitigate it with the ACt of the IC. Fig. 9(d)-(e) shows the S-parameter measurements of the amplitude calibration applied to the uniformly-fed broadside state represented within Fig. 9(a)-(c). This calibration is performed by only modifying the ACt of the IC to equalize all the output ports of the IC, while leaving the PCt applied in Fig. 9(a)-(c) unaltered. It can be appreciated that the amplitude transmission parameter $|S_{21}|$ per port referenced to the SW_HT port depicted in Fig. 9(d) has slightly changed compared to the previous state displayed in Fig. 9(a). The amplitude error among ports is now around ± 0.25 dB, which represents a much better result to obtain an amplitude distribution as uniform as possible at the active antenna aperture. Nevertheless, the original phase distribution portrayed in Fig. 9(b) has also been altered compared to the phase distribution depicted in Fig. 9(e). Although most of the phase states remains very similar compared to the phase configuration of the initial state depicted in Fig. 9(a)-(c), the phase state of the SE_VT port has been significantly changed. This channel presented the highest amplitude deviation for the initial state of the IC. This reveals a not negligible ACt/PCt (Amplitude Control to Phase Control) interaction effect on the IC transmission mechanism. This undesired alteration, which usually occurs in the amplification stage, modifies the transmission phase response when only the amplitude response is changed. This phenomenon may distort the proposed IC auto-calibration scheme. Moreover, the opposite PCt/ACt (Phase Control to Amplitude Control) interaction effect is also observed when trying to re-calibrate the phase distribution once the amplitude distribution has been modified. In this case, the phase-shifting step introduces an amplitude deviation in the transmission response when only the phase response is modified. It becomes clear that the IC is not able to self-calibrate its amplitude and phase errors at once for any possible configuration. The IC amplitude and phase transmissions are not independent and modifying one of them has an impact on the other, and with no control over it. Thus, a certain no auto-calibratable error will be assumed at the active antenna aperture. Additionally, the reflection parameters at the input and output ports along with the reverse amplitude transmission of the state depicted in Fig. 9(d)-(e) remains very similar with respect to the parameters displayed in Fig. 9(c).

Nevertheless, this amplitude and phase error levels will not significantly affect the radiation properties of the active antenna, as will be seen afterwards, regardless of how severe the ACt/PCt interaction effects are for a certain configuration. But for other radiating structures, that are capable of

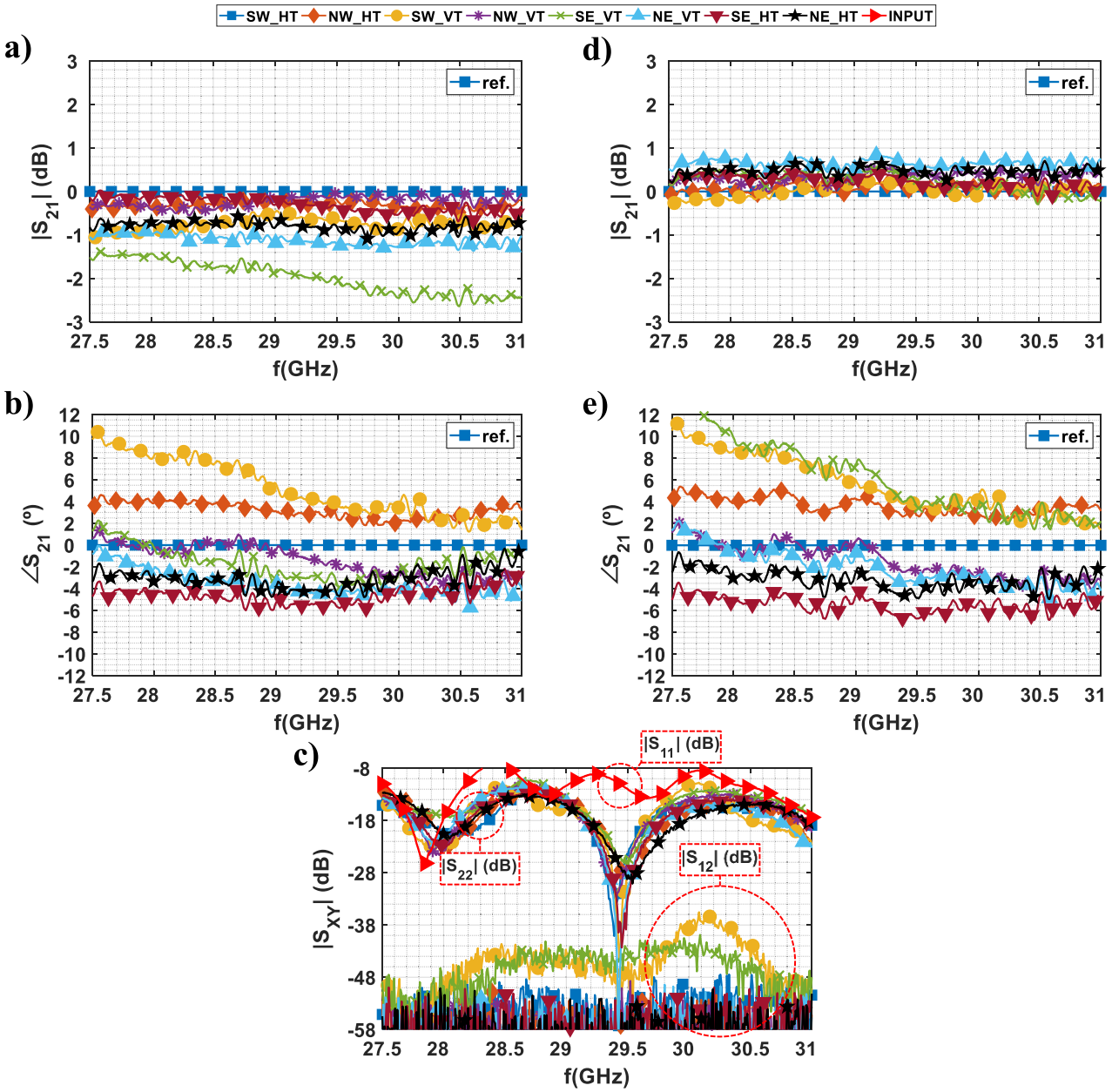

FIGURE 9. Measured Anokiwave AWMF-0109 broadside state: (a) amplitude transmission parameter $|S_{21}|$ per port referenced to SW_HT port, (b) phase transmission parameter $\angle S_{21}$ per port referenced to SW_HT port, and (c) reverse amplitude transmission parameter $|S_{12}|$ per port, reverse amplitude reflection parameter $|S_{22}|$ per port, and input reflection parameter $|S_{11}|$. Measured Anokiwave AWMF-0109 amplitude-calibrated broadside state: (d) amplitude transmission parameter $|S_{21}|$ per port referenced to SW_HT port, and (e) phase transmission parameter $\angle S_{21}$ per port referenced to SW_HT port.

generating switchable circular polarization, the assumed error and the no-calibration approach may not assess the viability of the system, at least for a single IC.

V. ACTIVE ARRAY ANTENNA MEASUREMENT

In this section, the integration procedure of the proposed array antenna and the IC-EB is addressed.

Prior to the integration stage, all the elements that represent a source of systematic phase and/or amplitude errors to the system in the integration process may be characterized to calibrate their responses with the IC. Components such as cables (which demonstrate high stability characteristics with bending), connector transitions or manufacture disparities on the feeding lines are taken into account in the performed calibration of the proof of concept. Unlike these systematic deviations suffered by the proposed system, which may be calibrated by the IC as accurate as possible, the IC errors are randomized due to the ACt/PCt and PCt/ACt interaction phenomena. These effects make it really difficult to equalize the amplitude and phase distribution by an auto-calibration

procedure as explained before. Hence, there is no other option but to assume them in the system. In addition, all these errors depend also on the frequency. Nevertheless, this dependency may be included into the calculation of the beam-steering direction, which is discussed within the next section. The behavior of the system against all the sources of amplitude and phase errors may reject or not the viability of the proposed analysis. As discussed within the previous sections, these issues do not affect the behavior of the proposed passive array antenna. For other type of antennas with different polarization schemes these errors will influence their radiation properties in such a different way that this viability assessment should be performed with them.

A. BEAM-STEERING DIRECTION CALCULATION FOR THE ACTIVE ANTENNA

When it comes to integrate both antenna and IC-EB, the calculation of the different phases per port to feed the antenna is discussed. As mentioned in the previous sections, the IC is capable of performing a 5-bit ACt and PCt over the transmission parameter S_{21} of each channel of the IC-EB. Therefore, there are 2^5 possible amplitude and 2^5 possible phase states for each transmission parameter. Hence, the number of all the different configurations of the IC is completely disproportionate, with a value of $8 \cdot 2^5 \cdot 2^5 = 8 \cdot 2^{10}$ different states. Due to this fact and to the discussed PCt/ACt and ACt/PCt interaction phenomena demonstrated at Section IV, it becomes unfeasible either to completely characterize the IC for all its possible configuration states or to calibrate the IC for each considered configuration. Moreover, this calibration process requires a re-calibration step (presumably more than one step) to adjust the amplitude when a particular set of phases is set or to adjust the phase when a particular set of amplitudes is set. Consequently, not only the discretization error in the phase will be assumed, but also the amplitude error that the particular phase distribution will generate due to the PCt/ACt interaction phenomenon. This assumed error is transferred to the antenna aperture and may degrade the generated radiation pattern. Nevertheless, it will be seen that this error does not affect the viability of the proposed system, but also helps to perform a smoother sweep when the pointing angle direction is changed.

For this analysis, a uniform amplitude distribution will be also considered. Thus, all the channels are set to their respective maximum gain state (see Fig. 2). Due to the PCt/ACt interaction effect of the IC this maximum gain states will vary with the phase distribution to point the active antenna to the required angle, and the amplitude difference between ports may be higher or lower depending on the configuration.

To calculate the progressive phase shifting φ between columns that is necessary to perform the steering of the beam towards the pointing angle direction θ, the expression used for a 1D linear array placed in the x-axis is utilized as $\varphi = k_0 \cdot dx \cdot \sin(\theta)$, where k_0 is the free-space wavenumber. Once the progressive phase shifting φ is calculated, each of the ports is set to the nearest phase state that preserves the previously mentioned relationship $\alpha_n = \alpha_0 - n \cdot \varphi$. To perform the PCt of the n-th column subarray to change its phase state α_n, the initial phase state δ_n of every channel is considered as the starting point and is associated to the nominal zero phase for any channel. This initial state δ_n per port is depicted in Fig. 9(b) referenced to SW_HT port, and it corresponds to the phase transmission parameter $\angle S_{21}^{(n)}$ of each port. The computed phase shift is rounded to the closest multiple of shf_{min}, where shf_{min} is the minimum phase step of the IC (11.25°), until the potential phase error in φ with respect to the previous column is minimized. The constant α_0 can be fixed to some specific value or adjusted for minimum discretization error at each pointing process, depending on the system interest of small phase jumping or computing capacity of the data processor. For other kind of passive antennas (e.g. the dual-polarized 2×2-element passive array for switchable circular polarization), the calculations would include not only the progressive phase shift φ for steering the beam, but also the 90° phase difference among dual ports to set the desired circular polarization. Thus, the potential amplitude and phase errors that would occur at the antenna aperture may impact differently on the antenna performance. Consequently it might happen that these errors cannot be assumed in the aperture, and another calibration strategy has to be applied (at least for antennas with a small number of elements).

Ideally, the parameter φ would not depend on the channel, the amplitude distribution, or the phase distribution, and should be constant between adjacent columns for each different configuration. However, and because of all the possible sources of error of the IC: amplitude discretization, phase discretization, PCt/ACt, and ACt/PCt interaction effects, the phase differences among channels will differ from the ideal distribution. Furthermore, depending on the considered phase distribution φ there will be some port phases further away from the expected than others. As previously mentioned, this discretization error will be assumed at the active antenna aperture. Moreover, all these errors will help the system to perform a smoother steering of the beam instead of a stepped steering of the beam. The root mean square error in φ is calculated for every considered configuration to quantify how much the amplitude and phase feeding coefficients are far from the ideal ones. In addition, for high beam-steered configurations the sidelobe level (SSL) is going to be increased due to the inclusion of the replicas of the main lobe in the visible region. Because of this, the maximum beam-steered configuration to analyze will be $\theta = \pm 50°$.

B. ACTIVE ARRAY ANTENNA MEASUREMENT RESULTS

In the current section all the measured radiation properties of the 8×8-element active array antenna are discussed. In Fig. 10 it can be shown the final prototype inside the anechoic chamber with all the RF, power and control interfaces connected to it.

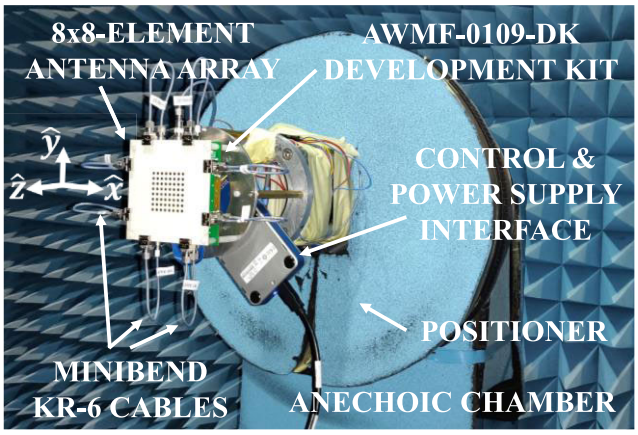

FIGURE 10. Active array antenna proof-of-concept within the anechoic chamber.

First of all, only 7 configurations of the antenna will be presented. They demonstrate the beam steering capabilities of the antenna for $\theta = \{0°, 5°, 10°, 20°, 30°, 40°, 50°\}$. All of them assume a uniform amplitude distribution with the inherent amplitude errors of the IC.

The measured copolar radiation patterns for the considered beam-steered configurations are shown in Fig. 11. The radiation patterns are only displayed for the middle frequency. However, the measured radiation patterns at the upper and lower frequencies exhibit a very similar behavior. It might be appreciated how the amplitude and phase imbalances impact on the radiation pattern by causing it to be asymmetrical. Nevertheless, these errors do not affect considerably to the radiation performance of the active antenna. All the radiation pattern asymmetries are reasonably low, and the influence of the array factor prevails.

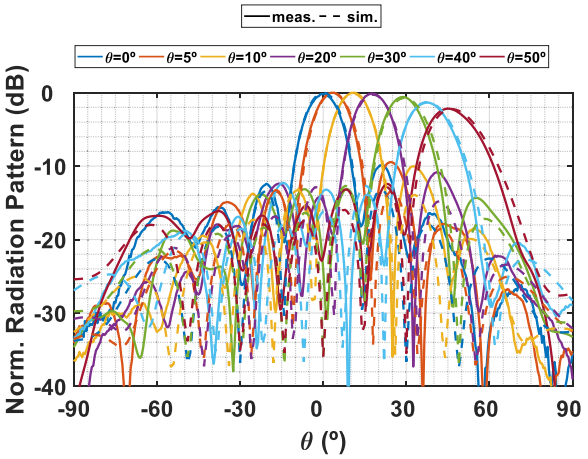

FIGURE 11. Simulated and measured copolar (CP) normalized radiation patterns for the beam-steered configurations of the active array antenna proof-of-concept.

In Fig. 12 it is depicted the Root Mean Square (RMS) error for the considered seven IC configurations. It evaluates how far are the measured S_{21} parameters for the 8 channels of the IC-EB with respect to the discretized ideal S_{21} parameters. Thus, the inherent IC imbalances are evaluated. It is well known that the associated gain reduction due to discretization depends strongly on the number of bits nbits and it is barely negligible when nbits ≥ 4 [51]. It can be seen that the amplitude RMS error and the phase RMS error remain below approximately 1 dB and 10° respectively. With these error levels, the impact on the gain decay is around 0.3-0.4 dB, and the pointing accuracy results outstanding. Hence, the viability of the proposed system is demonstrated. It is worth mentioning that the phase shifting approach of the IC is constant in phase, but not constant in delay (or True Time Delay (TTD)). Thus, the instantaneous bandwidth available for the transmitted signal is reduced. However, the frequency of the signal may be considered in the calculation of the steering of the beam, and consequently the transmission may be optimized.

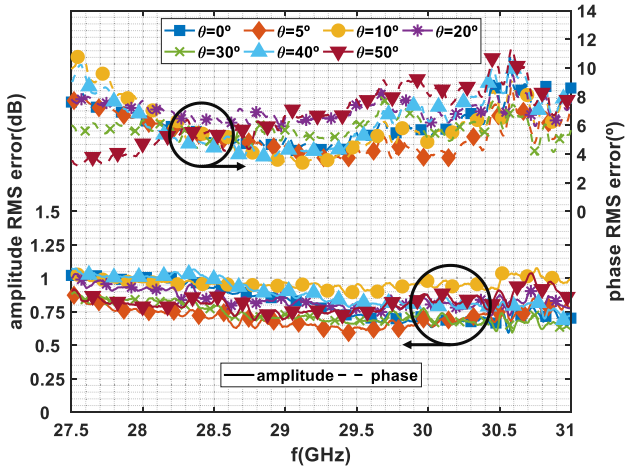

FIGURE 12. Amplitude and phase Root Mean Squared (RMS) errors of all the presented configurations between the measured and the ideal amplitude and phase distributions.

Additionally, in Fig. 11 the achieved accuracy between the expected pointing angle θ from the simulated and the measured results of the active array proves to be really precise. The error is negligible and below 1° for the most extreme case. This demonstrates a really good performance of the active array regarding the beam steering accuracy and assessing the viability of the proposed system and analysis approach. Besides, since the beamwidth of the active antenna is wide enough, the directivity difference between the simulated and measured results is also negligible.

Finally, in Fig. 13 it is depicted the maximum directivity achieved by each beam steering configuration of the active array. For the broadside state and the beam-steered directions close to it, the maximum directivity is very similar with a value around 22.3 dBi. For the directions farther from the broadside state this value begins to decay as expected. Nevertheless, it seems to be very stable within the frequency band. Since the complete system is an active device, the classic efficiency concept for passive antenna losses its meaning

and consequently, the gain concept has no interest except for interstate comparison [52]. Thus, and because the system under study is for transmission, an analysis of the maximum achievable Effective Isotropic Radiated Power (EIRP) is performed within the next section.

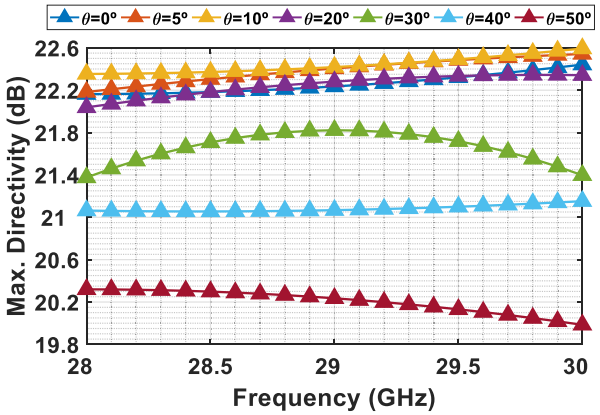

FIGURE 13. Measured maximum directivity achieved for every beam steering configuration of the active array.

C. EFFECTIVE ISOTROPIC RADIATED POWER (EIRP) ANALYSIS

As mentioned before, when dealing with active transmitting antennas, the Effective Isotropic Radiated Power (EIRP) that they can achieve becomes a very important Figure of Merit (FoM). In particular, the EIRP of the active antenna will be measured in the plane of the aperture for the broadside state. The measurement setup of the EIRP of the active antenna is very similar to that of Fig. 10. A Standard Gain Horn (SGH) is located in front of the active antenna placed in the probe positioner of the anechoic chamber. Besides, the gain of the SGH is accurately characterized to perform the EIRP calculation. The received power is measured at the interface of the anechoic chamber with the exterior. Thus, the losses of the RF chain between the measurement port and the SGH are also characterized for the EIRP calculation. So, the EIRP of the active antenna is extrapolated backwards with these data and the free-space losses occurring from the active antenna to the SGH. The received power measured from outside the anechoic chamber is sampled at 28, 29 and 30 GHz. This measurement approach is then validated at the active antenna side. The received power is sampled at the input port of the active array and then it is weighted by the maximum gain of the active array. The measurement results with both methods proved to be very similar, so the proposed EIRP measurement technique turned to be as accurate as expected.

Next, the active antenna EIRP is measured with all the channels of the IC at their maximum gain state, and the amplifier at the input branch with its attenuation level going from 15 dB to 2 dB (see Fig. 2). The EIRP measurement results for the considered frequencies are depicted in Fig. 14. All the displayed curves are reasonably linear until the attenuation level of 2 dB, where the IC seems to become unstable. Nevertheless, no saturation effects on the system are observed. Thus, a maximum achievable EIRP from 14 dBm to 20 dBm is demonstrated, depending on the operating frequency. The attenuation level of 1dB was not considered due to the power consumption demanded by the IC, which revealed a highly unstable behavior.

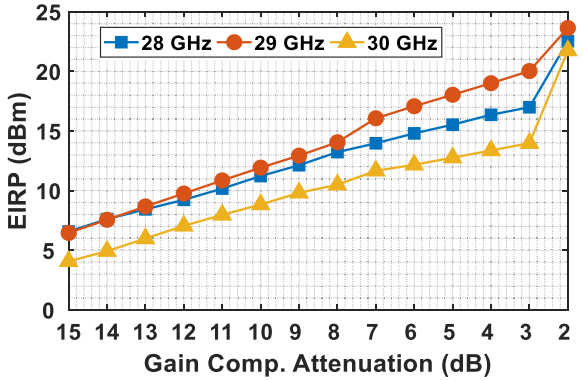

FIGURE 14. Effective Isotropic Radiated Power (EIRP) measurement results.

VI. CONCLUSION AND FURTHER RESEARCH

In this article, an 8 × 8-element active phased array antenna proof-of-concept for Ka band transmission applications is developed. The complete system consists of the integration of the AWMF-0109 IC from Anokiwave with a 8 × 8-element passive printed patch array antenna. This antenna is in turn divided into 8 1 × 8-element corporately-fed column subarrays. Thus, a beam steering control of the radiation pattern of the array is performed in the azimuth plane. The AWMF-0109 IC is characterized in terms of amplitude and phase error among output ports, which are different depending on the amplitude and phase distribution configuration of the IC. Additionally, all the components which mean a source of error for the system are calibrated within the IC properties.

Despite all the described errors present in the system, the control in the radiation properties of the array resulted really promising. The error on the beam-steered direction is always below 1°. Maximum EIRP value of the active array antenna goes from 14 dBm to 20 dBm depending on the operating frequency.

Further research steps will be to study the radiation properties of other passive array antennas to integrate with the IC, such as the previously mentioned dual-polarized 2 × 2-element array with switchable circular polarization capabilities. Therefore, the amplitude and phase errors of the IC that are assumed at the aperture could be analyzed within this structure to verify if any calibration step is required or not. These errors can drastically affect the performance of arrays with few elements, but for larger apertures this may not be critical. For this reason, circular patches were also used

within this work despite the polarization scheme was linear and not circular (and some other patch shapes may work better). This way, the performance of the IC in terms of axial ratio would be also tested. An additional research step would be to apply a formal mathematical analysis such as [47]–[50] to the IC that has been used. In this way, the behavior of the IC could be inferred and the active antenna calibration process would be possible. Our intention is also to measure a fully integrated antenna attaching the IC inside the antenna board to avoid line and connection losses and to obtain a real low profile planar antenna.

ACKNOWLEDGMENT

Simulations performed within this work have been done using CST Microwave Studio Suite 2019 under a cooperation agreement with Computer Simulation Technology (CST). The Authors would also like to recognize Anokiwave S. A. for the support provided to control and use their product.

REFERENCES

[1] Y.-B. Jung, S.-Y. Eom, and S.-I. Jeon, "Novel antenna system design for satellite mobile multimedia service," *IEEE Trans. Veh. Technol.*, vol. 59, no. 9, pp. 4237–4247, Nov. 2010.

[2] R. Baggen, S. Holzwarth, M. Bottcher, and S. Otto, "Innovative antenna front ends from L-band to Ka-band [antenna applications corner]," *IEEE Antennas Propag. Mag.*, vol. 59, no. 5, pp. 116–129, Oct. 2017.

[3] A. Jacomb-Hood and E. Lier, "Multibeam active phased arrays for communications satellites," *IEEE Microw. Mag.*, vol. 1, no. 4, pp. 40–47, Dec. 2000.

[4] M. Khalily, R. Tafazolli, P. Xiao, and A. A. Kishk, "Broadband mm-wave microstrip array antenna with improved radiation characteristics for different 5G applications," *IEEE Trans. Antennas Propag.*, vol. 66, no. 9, pp. 4641–4647, Sep. 2018.

[5] M. Ikram, E. A. Abbas, N. Nguyen-Trong, K. H. Sayidmarie, and A. Abbosh, "Integrated frequency-reconfigurable slot antenna and connected slot antenna array for 4G and 5G mobile handsets," *IEEE Trans. Antennas Propag.*, vol. 67, no. 12, pp. 7225–7233, Dec. 2019.

[6] D. Liu, X. Gu, C. W. Baks, and A. Valdes-Garcia, "Antenna-in-package design considerations for Ka-band 5G communication applications," *IEEE Trans. Antennas Propag.*, vol. 65, no. 12, pp. 6372–6379, Dec. 2017.

[7] G. Menon, R. Mcmorrow, and D. Corman, "Active antennas for emerging X-band RADAR applications," in *Proc. IEEE Radar Conf. (RadarConf)*, Oklahoma City, OK, USA, Apr. 2018, pp. 1334–1337.

[8] A. Dubok, A. Al-Rawi, N. Tessema, E. Tangdiongga, M. H. A. J. Herben, G. Gerini, and A. B. Smolders, "Double-reflector configuration for optimal exposure of wideband focal-plane arrays with optical beamforming," *IEEE Trans. Antennas Propag.*, vol. 65, no. 8, pp. 4316–4321, Aug. 2017.

[9] N. J. G. Fonseca, E. Girard, and H. Legay, "Doubly curved reflector design for hybrid array fed reflector antennas," *IEEE Trans. Antennas Propag.*, vol. 66, no. 4, pp. 2079–2083, Apr. 2018.

[10] A. Dubok, A. Al-Rawi, G. Gerini, and A. B. Smolders, "Reflector synthesis for wide-scanning focal plane arrays," *IEEE Trans. Antennas Propag.*, vol. 67, no. 4, pp. 2305–2319, Apr. 2019.

[11] Y.-B. Jung, A. V. Shishlov, and S.-O. Park, "Cassegrain antenna with hybrid beam steering scheme for mobile satellite communications," *IEEE Trans. Antennas Propag.*, vol. 57, no. 5, pp. 1367–1372, May 2009.

[12] S. Y. Eom, S. H. Son, Y. B. Jung, S. I. Jeon, S. A. Ganin, A. G. Shubov, A. K. Tobolev, and A. V. Shishlov, "Design and test of a mobile antenna system with tri-band operation for broadband satellite communications and DBS reception," *IEEE Trans. Antennas Propag.*, vol. 55, no. 11, pp. 3123–3133, Nov. 2007.

[13] K. K. Karnati, Y. Shen, M. E. Trampler, S. Ebadi, P. F. Wahid, and X. Gong, "A BST-integrated capacitively loaded patch for K_a- and X-band beamsteerable reflectarray antennas in satellite communications," *IEEE Trans. Antennas Propag.*, vol. 63, no. 4, pp. 1324–1333, Apr. 2015.

[14] Q. Luo, S. Gao, C. Zhang, D. Zhou, T. Chaloun, W. Menzel, V. Ziegler, and M. Sobhy, "Design and analysis of a reflectarray using slot antenna elements for Ka-band SatCom," *IEEE Trans. Antennas Propag.*, vol. 63, no. 4, pp. 1365–1374, Apr. 2015.

[15] X. Zhang, F. Yang, S. Xu, and M. Li, "Single-layer reflectarray antenna with independent dual-CP beam control," *IEEE Antennas Wireless Propag. Lett.*, vol. 19, no. 4, pp. 532–536, Apr. 2020.

[16] T. Chaloun, V. Ziegler, and W. Menzel, "Design of a dual-polarized stacked patch antenna for wide-angle scanning reflectarrays," *IEEE Trans. Antennas Propag.*, vol. 64, no. 8, pp. 3380–3390, Aug. 2016.

[17] P. Nayeri, F. Yang, and A. Z. Elsherbeni, "Bifocal design and aperture phase optimizations of reflectarray antennas for wide-angle beam scanning performance," *IEEE Trans. Antennas Propag.*, vol. 61, no. 9, pp. 4588–4597, Sep. 2013.

[18] T. Chaloun, C. Hillebrand, C. Waldschmidt, and W. Menzel, "Active transmitarray submodule for K/Ka band satcom applications," in *Proc. German Microw. Conf.*, Nuremberg, Germany, Mar. 2015, pp. 198–201.

[19] L. Di Palma, A. Clemente, L. Dussopt, R. Sauleau, P. Potier, and P. Pouliguen, "Circularly-polarized reconfigurable transmitarray in Ka-band with beam scanning and polarization switching capabilities," *IEEE Trans. Antennas Propag.*, vol. 65, no. 2, pp. 529–540, Feb. 2017.

[20] S. A. Matos, E. B. Lima, J. S. Silva, J. R. Costa, C. A. Fernandes, N. J. G. Fonseca, and J. R. Mosig, "High gain dual-band beam-steering transmit array for satcom terminals at Ka-band," *IEEE Trans. Antennas Propag.*, vol. 65, no. 7, pp. 3528–3539, Jul. 2017.

[21] K. T. Pham, R. Sauleau, E. Fourn, F. Diaby, A. Clemente, and L. Dussopt, "Dual-band transmitarrays with dual-linear polarization at Ka-band," *IEEE Trans. Antennas Propag.*, vol. 65, no. 12, pp. 7009–7018, Dec. 2017.

[22] G. Liu, M. R. D. Kodnoeih, K. T. Pham, E. M. Cruz, D. Gonzalez-Ovejero, and R. Sauleau, "A millimeter-wave multibeam transparent transmitarray antenna at Ka-band," *IEEE Antennas Wireless Propag. Lett.*, vol. 18, no. 4, pp. 631–635, Apr. 2019.

[23] J. S. Silva, E. B. Lima, J. R. Costa, C. A. Fernandes, and J. R. Mosig, "Tx-Rx lens-based satellite-on-the-move Ka-band antenna," *IEEE Antennas Wireless Propag. Lett.*, vol. 14, pp. 1408–1411, 2015.

[24] A. A. Baba, R. M. Hashmi, K. P. Esselle, M. Attygalle, and D. Borg, "A millimeter-wave antenna system for wideband 2-D beam steering," *IEEE Trans. Antennas Propag.*, vol. 68, no. 5, pp. 3453–3464, May 2020.

[25] E. B. Lima, S. A. Matos, J. R. Costa, C. A. Fernandes, and N. J. G. Fonseca, "Circular polarization wide-angle beam steering at Ka-band by in-plane translation of a plate lens antenna," *IEEE Trans. Antennas Propag.*, vol. 63, no. 12, pp. 5443–5455, Dec. 2015.

[26] H.-F. Wang, Z.-B. Wang, Z.-H. Wu, and Y.-R. Zhang, "Beam-scanning lens antenna based on elliptical paraboloid phase distribution metasurfaces," *IEEE Antennas Wireless Propag. Lett.*, vol. 18, no. 8, pp. 1562–1566, Aug. 2019.

[27] Y.-Y. Lin, C.-L. Liao, T.-H. Hsieh, and W.-J. Liao, "A novel beam-switching array antenna using series-fed slots with PIN diodes," *IEEE Antennas Wireless Propag. Lett.*, vol. 16, pp. 1393–1396, 2017.

[28] E. Ojefors, S. Cheng, K. From, I. Skarin, P. Hallbjorner, and A. Rydberg, "Electrically steerable single-layer microstrip traveling wave antenna with varactor diode based phase shifters," *IEEE Trans. Antennas Propag.*, vol. 55, no. 9, pp. 2451–2460, Sep. 2007.

[29] T. Lambard, O. Lafond, M. Himdi, H. Jeuland, S. Bolioli, and L. Le Coq, "Ka-band phased array antenna for high-data-rate SATCOM," *IEEE Antennas Wireless Propag. Lett.*, vol. 11, pp. 256–259, 2012.

[30] J. Zhou, L. Yin, L. Kang, M. Wang, and J. Huang, "Joint design and experimental tests of highly integrated phased-array antenna with microchannel heat sinks," *IEEE Antennas Wireless Propag. Lett.*, vol. 18, no. 11, pp. 2370–2374, Nov. 2019.

[31] Q.-Q. He, S. Ding, C. Xing, J.-Q. Chen, G.-Q. Yang, and B.-Z. Wang, "Research on structurally integrated phased array for wireless communications," *IEEE Access*, vol. 8, pp. 52359–52369, 2020.

[32] H. Al-Saedi, W. M. Abdel-Wahab, S. M. Raeis-Zadeh, E. H. M. Alian, A. Palizban, A. Ehsandar, N. Ghafarian, G. Chen, S. R. Boroujeni, M.-R. Nezhad-Ahmadi, and S. Safavi-Naeini, "An integrated circularly polarized transmitter active phased-array antenna for emerging Ka-band satellite mobile terminals," *IEEE Trans. Antennas Propag.*, vol. 67, no. 8, pp. 5344–5352, Aug. 2019.

[33] L. Baggen, S. Vaccaro, D. L. del Rio, and J. Padilla, "A compact phased array for satcom applications," in *Proc. IEEE Int. Symp. Phased Array Syst. Technol.*, Boston, MA, USA, Oct. 2013, pp. 232–239.

[34] W. Theunissen, V. Jain, and G. Menon, "Development of a receive phased array antenna for high altitude platform stations using integrated beamformer modules," in *IEEE MTT-S Int. Microw. Symp. Dig.*, Philadelphia, PA, USA, Jun. 2018, pp. 779–782.
[35] M. Stoneback and K. Madsen, "A planar all-silicon 256-element Ka-band phased array for high-altitude platforms (HAPs) application," in *IEEE MTT-S Int. Microw. Symp. Dig.*, Jun. 2018, pp. 783–786.
[36] W. M. Abdel-Wahab, H. Al-Saedi, E. H. M. Alian, M. Raeis-Zadeh, A. Ehsandar, A. Palizban, N. Ghafarian, G. Chen, H. Gharaee, M. R. Nezhad-Ahmadi, and S. S. Naeini, "A modular architecture for wide scan angle phased array antenna for K/Ka mobile SATCOM," in *IEEE MTT-S Int. Microw. Symp. Dig.*, Boston, MA, USA, Jun. 2019, pp. 1076–1079.
[37] A. I. Sandhu, E. Arnieri, G. Amendola, L. Boccia, E. Meniconi, and V. Ziegler, "Radiating elements for shared aperture Tx/Rx phased arrays at K/Ka band," *IEEE Trans. Antennas Propag.*, vol. 64, no. 6, pp. 2270–2282, Jun. 2016.
[38] C.-Y. Chu, Y.-P. Chen, J.-Z. Gao, C.-Y. Ke, Y.-W. Chen, L.-H. Chang, B. Su, T.-S. Chu, and Y.-J. Wang, "A Ka-band scalable hybrid phased array based on four-element ICs," *IEEE Trans. Microw. Theory Techn.*, vol. 68, no. 1, pp. 288–300, Jan. 2020.
[39] K. Kibaroglu, M. Sayginer, T. Phelps, and G. M. Rebeiz, "A 64-element 28-GHz phased-array transceiver with 52-dBm EIRP and 8–12-Gb/s 5G link at 300 meters without any calibration," *IEEE Trans. Microw. Theory Techn.*, vol. 66, no. 12, pp. 5796–5811, Dec. 2018.
[40] H. Schumacher, M. Kaynak, V. Valenta, and B. Tillack, "Smarter ICs," *IEEE Microw. Mag.*, vol. 13, no. 7, pp. S33–S40, Nov. 2012.
[41] S. Dubal and A. Chaudhari, "Mechanisms of reconfigurable antenna: A review," in *Proc. 10th Int. Conf. Cloud Comput., Data Sci. Eng. (Confluence)*, Noida, India, Jan. 2020, pp. 576–580.
[42] O. Bayraktar, E. Kobal, Y. Sevinc, C. Cetintepe, I. Comart, K. Demirel, E. S. Topalli, T. Akin, S. Demir, and O. A. Civi, "RF MEMS based millimeter wave phased array for short range communication," in *Proc. 9th Eur. Conf. Antennas Propag. (EuCAP)*, Lisbon, Portugal, 2015, pp. 1–5.
[43] W. Gautier, V. Ziegler, A. Stehle, B. Schoenlinner, U. Prechtel, and W. Menzel, "RF-MEMS phased array antenna on low-loss LTCC substrate for Ka-band data link," in *Proc. Eur. Microw. Conf. (EuMC)*, vol. 1, Oct. 2009, pp. 914–917.
[44] R. Malmqvist, C. Samuelsson, P. Rantakari, T. Vaha-Heikkila, D. Smith, J. Varis, and R. Baggen, "RF MEMS and MMIC based reconfigurable matching networks for adaptive multi-band RF front-ends," in *Proc. IEEE Int. Microw. Workshop Ser. RF Front-Ends Softw. Defined Cognit. Radio Solutions (IMWS)*, Aveiro, Portugal, Feb. 2010, pp. 1–4.
[45] B.-W. Min and G. M. Rebeiz, "Single-ended and differential Ka-band BiCMOS phased array front-ends," *IEEE J. Solid-State Circuits*, vol. 43, no. 10, pp. 2239–2250, Oct. 2008.
[46] Y. P. Zhang and D. Liu, "Antenna-on-chip and antenna-in-package solutions to highly integrated millimeter-wave devices for wireless communications," *IEEE Trans. Antennas Propag.*, vol. 57, no. 10, pp. 2830–2841, Oct. 2009.
[47] R. Zaker, A. Abdipour, A. Tavakoli, and R. Mirzavand, "Frequency-dependent behavioral-model-based nonlinear analysis and design of a low-profile transmit active phased array antenna," *Int. J. RF Microw. Comput.-Aided Eng.*, vol. 28, no. 6, pp. 1–14, Aug. 2018.
[48] K. J. Maalouf and E. Lier, "Theoretical and experimental study of interference in multibeam active phased array transmit antenna for satellite communications," *IEEE Trans. Antennas Propag.*, vol. 52, no. 2, pp. 587–592, Feb. 2004.
[49] C. Fager, X. Bland, K. Hausmair, J. C. Cahuana, and T. Eriksson, "Prediction of smart antenna transmitter characteristics using a new behavioral modeling approach," in *IEEE MTT-S Int. Microw. Symp. Dig.*, Tampa, FL, USA, Jun. 2014, pp. 1–4.
[50] G. Z. El Nashef, F. Torres, S. Mons, T. Reveyrand, T. Monediere, E. Ngoya, and R. Quere, "EM/circuit mixed simulation technique for an active antenna," *IEEE Antennas Wireless Propag. Lett.*, vol. 10, pp. 354–357, 2011.
[51] R. C. Hansen, "Basic array characteristics," in *Phased Array Antennas*, 2nd ed. Hoboken, NJ, USA: Wiley, 2009, ch. 2, secs. 2–4, pp. 28–32.
[52] R. J. Mailloux, "Phased arrays in radar and communication systems," in *Phased Array Antenna Handbook* (Artech House Antennas and Propagation Library), 2nd ed. Norwood, MA, USA: Artech House, 2005, ch. 1, secs. 1–2, pp. 35–37.

ALFONSO TOMÁS MURIEL-BARRADO was born in Madrid, Spain, in 1990. He received the M.Sc. degree in telecommunication engineering from the Universidad Autónoma de Madrid (UAM), Spain, in 2015. He is currently pursuing the Ph.D. degree with the Universidad Politécnica de Madrid (UPM). In February 2020, he joined UAM, as an Adjunct Professor. He is also the part of the Grupo de Radiación (GR) Research Group, UPM. His current research interest includes design and prototyping of planar array antennas in different technologies and their migration to beam-steered systems by means of different radiofrequency/microwave circuitry.

JORGE CALATAYUD-MAESO (Student Member, IEEE) was born in Madrid, Spain, in 1997. He received the B.Sc. degree in telecommunication technologies and services engineering from the Universidad Politécnica de Madrid (UPM), Spain, in 2019, where he is currently pursuing the M.Sc. degree in telecommunication engineering. He is also working as a Research Assistant with the Grupo de Radiación (GR) Research Group, UPM. His research interests include control systems for RF applications, planar array antenna design, manufacture and measurement, and compact antenna test range (CATR) measurement systems.

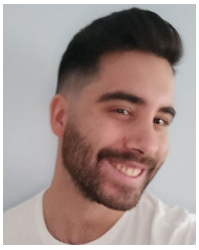

ANTONIO RODRÍGUEZ-GALLEGO was born in Madrid, Spain, in 1996. He received the B.Sc. degree in telecommunication technologies and services engineering and the M.Sc. degree in telecommunication engineering from the Universidad Politécnica de Madrid (UPM), Spain, in 2018 and 2020, respectively. Since 2020, he has been working as a Radar Engineer with Indra Sistemas S.A, Madrid. His current research interests include design and prototyping of planar array antennas, phased array antennas, and waveguide antennas.

PABLO SÁNCHEZ-OLIVARES was born in Madrid, Spain, in 1987. He received the degree in telecommunication engineering and the Ph.D. degree from the Universidad Autonoma de Madrid (UAM), Spain, in 2011 and 2018, respectively. From 2018 to 2019, he was worked as an Adjunct Professor with UAM, and a Postdoctoral Researcher Associate with the Universidad de Alcalá de Henares (UAH). Since 2019, he has been an Assistant Professor with the Universidad Politécnica de Madrid (UPM). His current research interests include the design, manufacturing and measurement of planar array antennas, phased array antennas, and waveguide antennas.

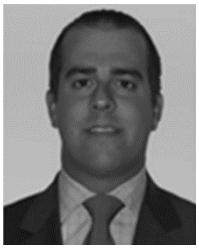

JOSÉ MANUEL FERNÁNDEZ-GONZÁLEZ (Senior Member, IEEE) was born in Lausanne, Switzerland. He received the Diplôme d'Ingénieur en Électricité degree from the École Polytechnique Fédérale de Lausanne, Lausanne, in 2003, and the Ph.D. degree from the Universidad Politécnica de Madrid, Madrid, Spain, in 2009. In 2006, he joined the Centre de Recherches Poly-Grames, l'École Polytechnique de Montréal, Montreal, QC, Canada, and the Chalmers University of Technology, Göteborg, Sweden, as a Guest Ph.D. Student, in 2007. From 2013 to 2019, he was an Assistant Professor with the Universidad Politécnica de Madrid. In 2018, he was a Fulbright Visiting Researcher with the Antenna Research Group, University of Colorado at Boulder. Since 2019, he has been an Associate Professor with the Universidad Politécnica de Madrid. He has participated in more than 35 research projects and contracts. He has authored more than 90 publications in scientific journals, symposium proceedings, and seminars, and holds four patents. His current research interests include phased array antennas, RF circuits, and metamaterial structures with emphasis on planar antenna applications.

MANUEL SIERRA-PÉREZ (Life Senior Member, IEEE) was born in Zaragoza, Spain, in 1952. He received the master's degree and the Ph.D. degree from the Universidad Politécnica de Madrid (UPM), in 1975 and 1980, respectively. He was an Invited Professor with the National Radio-Astronomy Observatory (NRAO), USA, from 1981 to 1982, and the University of Colorado at Boulder, from 1994 to 1995. In 1990, he became a Full Professor with the Department of Signals, Systems and Radio-communications, UPM. He is currently an Emeritus Professor with UPM. His current main interest is in passive and active array antennas, including design theory, measurement, and applications. His main research interest includes in the design and measurement of active antenna arrays. He was a Promoter and the Chairman of the IEEE Joint AP/MTT Spanish Chapter. He has been the Chairman of the IEEE Spain Section, the President of Spain antenna network and Spanish delegate on the European Association on Antennas and Propagation (EurAAP) Assembly.